

Using Postsynthetic X-Type Ligand Exchange to Enhance CO₂ Adsorption in Metal–Organic Frameworks with Kuratowski-Type Building Units

Caitlin E. Bien,[†] Zhongzheng Cai,[†] and Casey R. Wade*[‡]



Cite This: <https://doi.org/10.1021/acs.inorgchem.1c01077>



Read Online

ACCESS |



Metrics & More

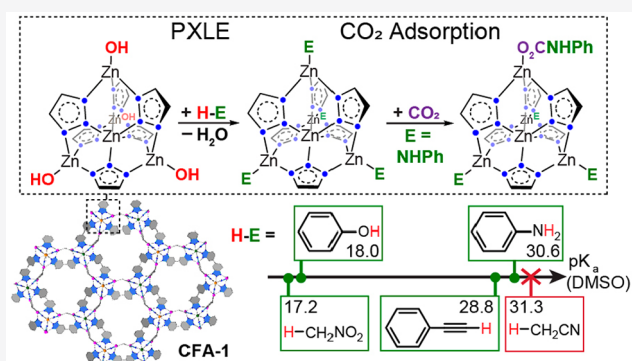


Article Recommendations



Supporting Information

ABSTRACT: Postsynthetic modification methods have emerged as indispensable tools for tuning the properties and reactivity of metal–organic frameworks (MOFs). In particular, postsynthetic X-type ligand exchange (PXLE) at metal building units has gained increasing attention as a means of immobilizing guest species, modulating the reactivity of framework metal ions, and introducing new functional groups. The reaction of a Zn–OH functionalized analogue of CFA-1 (1-OH, Zn(ZnOH)₄(bibta)₃, where bibta²⁻ = 5,5'-bibenzotriazolate) with organic substrates containing mildly acidic E–H groups (E = C, O, N) results in the formation of Zn–E species and water as a byproduct. This Brønsted acid–base PXLE reaction is compatible with substrates with pK_a(DMSO) values as high as 30 and offers a rapid and convenient means of introducing new functional groups at Kuratowski-type metal nodes. Gas adsorption and diffuse reflectance infrared Fourier transform spectroscopy experiments reveal that the anilide-exchanged MOFs 1-NHPh_{0.9} and 1-NHPh_{2.5} exhibit enhanced low-pressure CO₂ adsorption compared to 1-OH as a result of a Zn–NHPh + CO₂ ⇌ Zn–O₂CNHPh chemisorption mechanism. The MFU-4l analogue 2-NHPh ([Zn₂(OH)_{2.1}(NHPh)_{1.9}(btdd)₃], where btdd²⁻ = bis(1,2,3-triazolo)dibenzodioxin), shows a similar improvement in CO₂ adsorption in comparison to the parent MOF containing only Zn–OH groups.



INTRODUCTION

The past two decades have witnessed tremendous growth in the study of metal–organic frameworks (MOFs) as they have permeated nearly every chemical subfield and continued to spark the scientific imagination.^{1,2} Their modularity and astounding porosity have propelled the synthesis of thousands of new structures for fundamental studies and potential applications in gas storage and separation,^{3–6} catalysis,^{7–9} drug delivery,¹⁰ energy storage and electronic devices,^{11,12} and a host of others. MOFs represent a bridge between homogeneous, molecular chemistry and solid-state materials but offer more than a simple translation of the molecular properties. Indeed, new or unexpected properties often arise from the framework microenvironment and site isolation.^{13–24}

Postsynthetic modification (PSM) has emerged as an essential tool for tuning the properties and reactivity of MOFs.^{25–29} A variety of different PSM methods have been developed, but they share the common objective of furnishing MOFs with structural or chemical features that are not readily accessible using direct synthetic methods. PSM methods can be broadly categorized by the type of reaction (exchange, removal, and addition/insertion) and target component (linker or metal node) (Figure 1). Exchange reactions in which structural components (linkers or metal ions) are replaced

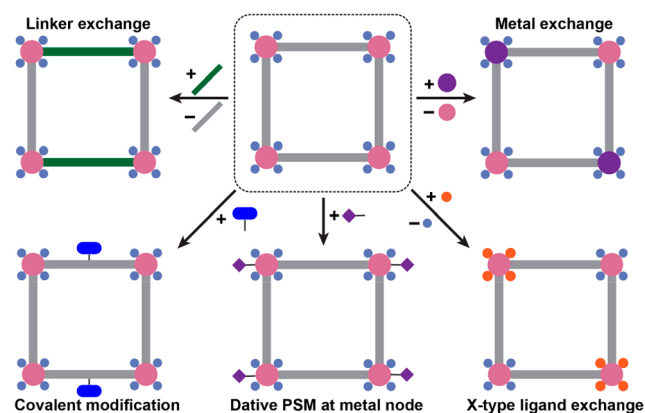


Figure 1. Summary of common PSM methods.

Special Issue: Postsynthetic Modification of Metal–Organic Frameworks

Received: April 7, 2021

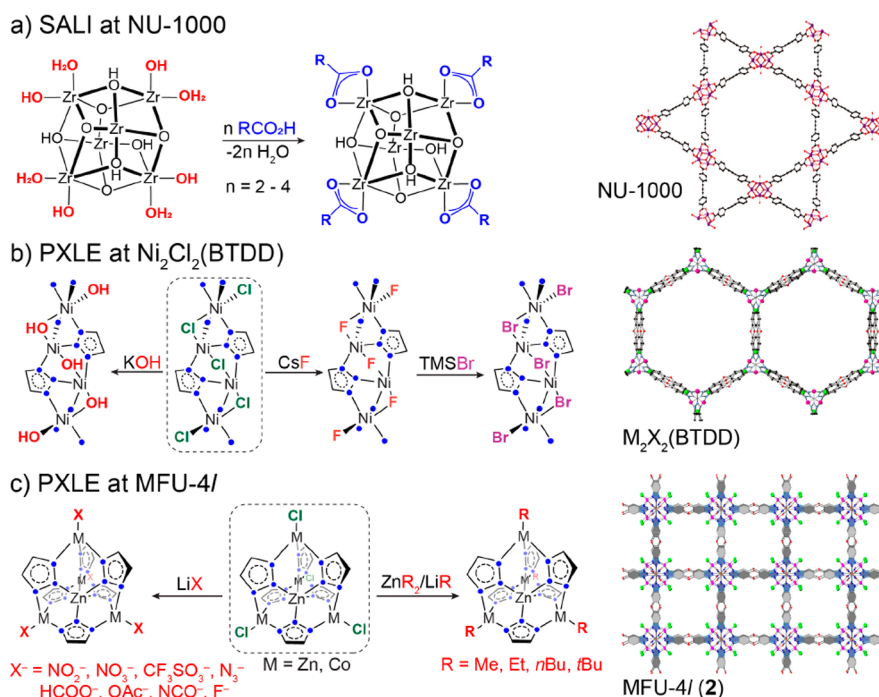


Figure 2. Selected examples of PXLE.^{64,83,93,100}

without dissolution of the framework have been developed to the point that they are now routine. Postsynthetic metal exchange (PSME) provides access to metal nodes with variable bi- or multimetallic compositions.^{30,31} Similarly, linker exchange allows for substitution using extrinsic linkers of similar size or shape but varying ancillary functional groups.^{32,33} Heterogeneous reactions can also be performed at organic linkers or metal nodes to insert new functional groups or modify existing ones. Covalent modification of organic linkers remains one of the most common and straightforward methods of inserting new functional groups.³⁴ This approach usually relies on linkers with reactive groups such as amines or aldehydes and benefits from well-established synthetic organic methods.

PSM of MOFs by removal or exchange of ancillary ligands at metal nodes is also quite common. The most prevalent example is the removal of nonstructural L-type ligands (e.g., water or *N,N*-dimethylformamide) using heat and/or vacuum.³⁵ The resulting Lewis acidic, coordinatively unsaturated metal sites have become a hallmark functional group for MOF-based adsorbents and catalysts.³⁶ Labile solvent ligands can also be exchanged to graft new functional groups at metal nodes. One of the earliest examples of this approach involved the substitution of axial aqua ligands with pyridine at the dicopper paddlewheel nodes of HKUST-1.³⁷ L-type ligand exchange or “dative PSM” at metal nodes has subsequently been employed to immobilize species that modify the guest adsorption properties,^{38,39} introduce chirality,^{40,41} or serve as catalytically active sites.^{42,43} Recently, diamine-grafted MOFs have received considerable attention as adsorbents for selective CO₂ capture.^{44–52} Most notably, Long and co-workers have shown that amine-grafted variants of Mg₂(dobpdc) [dobpdc⁴⁻ = 4,4′-dihydroxy-(1,1′-biphenyl)-3,3′-dicarboxylate] exhibit step-like CO₂ adsorption, resulting from a cooperative chemisorption mechanism.⁵³ Carbamate formation via CO₂ insertion into an Mg–N bond is accompanied by proton transfer to a neighboring diamine ligand, and this process

propagates to form one-dimensional ammonium carbamate chains.

There are numerous examples of postsynthetic exchange of charge-balancing anions residing within the pores of cationic MOFs.^{54–63} However, inner-sphere, postsynthetic X-type ligand exchange (PXLE) at MOF metal nodes has been less studied, partly as a result of the relative paucity of materials containing exchangeable X-type ligands. Hupp and co-workers pioneered solvent-assisted ligand incorporation (SALI) as a means of immobilizing nonstructural carboxylate or phosphonate groups at linker-deficient 6- or 8-connected Zr₆ nodes (Figure 2a).⁶⁴ The method relies on acid–base chemistry to substitute terminal OH⁻/H₂O ligands at Zr sites of the nodes, and the mild conditions have allowed for the immobilization of a wide range of functional molecules.^{65–71} Yaghi and co-workers have used a similar PXLE approach to bind small molecules at the Al-based metal nodes of chiral MOF-520. The immobilization method, termed coordinative alignment, reduces the degrees of freedom of the guest species and facilitates structural characterization via single-crystal X-ray diffraction of MOF crystals.^{72,73} Linker installation or “retrofitting” strategies involving PXLE at undercoordinated Zr or Al metal nodes bearing labile monotopic ligands have also been developed.^{18,74,75}

MOFs assembled from bis(benzotriazolate) linkers have also emerged as platforms for using PXLE to modify gas adsorption and catalytic properties. The high donor atom to charge ratio of the benzotriazolate groups tends to favor the formation of Kuratowski- or chain-type metal nodes with charge compensating anions. M₂X₂(BBTA) (BBTA²⁻ = benzo(1,2-*d*:4,5-*d'*)-bistriazolate) and M₃X₂(BTDD) [BTDD²⁻ = bis(1,2,3-triazolato)dibenzodioxin] adopt honeycomb structures with chains of metal ions coordinated by three benzotriazolate nitrogen atoms, two bridging halide or hydroxide anions (X), and a terminal solvent ligand (Figure 2b).^{76–78} Li and co-workers showed that PXLE of the μ-Cl⁻ ligands in Co₂Cl₂(BBTA) (MAF-X27-Cl) for μ-OH⁻ results in improved

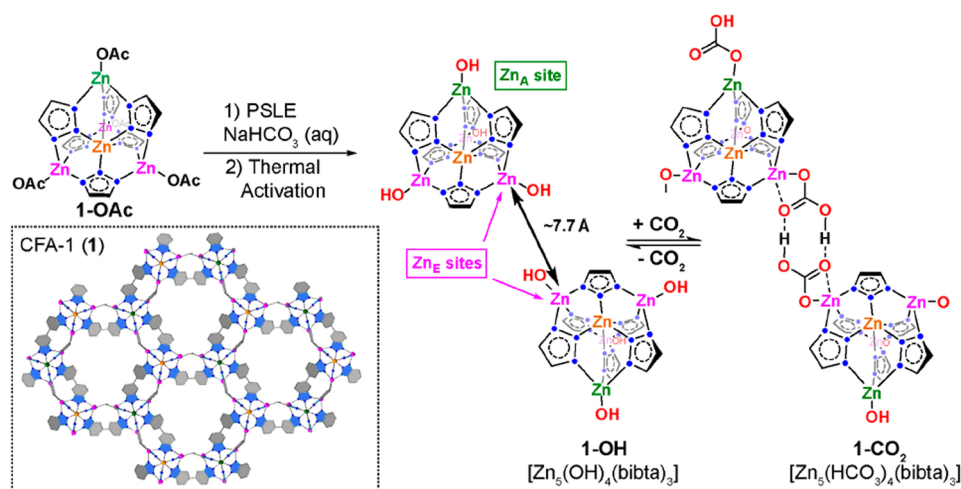


Figure 3. Postsynthetic ligand exchange of Zn–OAc to generate Zn–OH in **1-OAc** and reversible CO₂ binding.

electrocatalytic activity toward water oxidation.⁷⁹ Subsequent reports from the groups of Snurr and Long showed that Co₂(μ-OH)₂(BBTA) strongly chemisorbs O₂ at the coordinatively unsaturated Co²⁺ sites, while Co₂Cl₂(BBTA) exhibits only weak O₂ physisorption.^{80,81} A concurrent density functional theory (DFT) computational study explored how varying the bridging anion in the M₂X₂(BBTA) series of MOFs could be used to optimize the reactivity of putative metal–oxo species toward C–H bond activation.⁸² Dincă and co-workers have also used PXLE to prepare a series of anion-exchanged variants of Ni₂X₂BTDD (X = Cl, F, Br, OH) and investigate the effect of bridging anion identity on the hydrophobicity and water adsorption properties (Figure 2b).⁸³ The resulting materials showed remarkable differences in the relative humidity at which the water adsorption steps occurred.

The zinc benzotriazolate MOFs MFU-4, MFU-4l, and CFA-1 (CFA = Coordination Framework Augsburg University and MFU = Metal–organic Framework Ulm University) are assembled from discrete [Zn₃X₄(bt)₆] metal nodes (X[−] = Cl[−], CH₃CO₂[−]; bt[−] = benzotriazolate), also referred to as Kuratowski clusters.^{84–86} Each node is comprised of an octahedrally coordinated, central Zn site and four peripheral metal sites in pseudotetrahedral coordination geometries capped by a terminal X-type ligand (Figure 2c). These materials are chemically and thermally robust and highly amenable to postsynthetic metal and ligand exchange. As a result, PSM methods have been used to elaborate this small family of MOFs as catalysts for olefin polymerization^{87–92} and C–H bond oxidation^{93,94} as well as adsorbents for selective CO₂ and olefin capture.^{95–99} In an early study, Volkmer and co-workers screened PXLE reactions at the terminal Co–Cl sites of Co^{II}-exchanged MFU-4l using alkali metal salts to carry out anion metathesis.⁹³ Nearly complete substitution occurred with a variety of different anions, including NO₂[−], NO₃[−], N₃[−], NCO[−], HCO₂[−], and F[−]. More recently, the same group showed that organozinc and organolithium reagents could be used to functionalize the peripheral Zn/Co sites of MFU-4l with alkyl and acetylide ligands.¹⁰⁰ PXLE reactions in MFU-4l have also facilitated subsequent modifications and new types of reactivity. For example, thermolysis of MFU-4l analogues containing Zn–O₂CH and Cu–O₂CH groups was found to generate Zn–H and coordinatively unsaturated Cu^I sites, respectively.¹⁰¹ The latter were shown to strongly bind small

molecules such as O₂, N₂, and H₂. Cu^I-MFU-4l has also recently been exploited for olefin separation^{98,99} and NO disproportionation.¹⁰²

Recently, our group and others have used PXLE to generate nucleophilic transition-metal hydroxide groups (M–OH, where M = Co, Zn, and Ni) at the peripheral metal sites of CFA-1, MFU-4, and MFU-4l.^{95–97,103} The resulting M–OH species resemble the active sites of α-carbonic anhydrases and are highly reactive, allowing the MOFs to adsorb large amounts of CO₂ at low partial pressures via a M–OH + CO₂ ⇌ M–O₂COH chemisorption mechanism. The CO₂ capacity and isosteric heat of adsorption in these materials can be modulated by using PSME to vary the metal composition.⁹⁶ In addition, spectroscopic data and computational studies have revealed that inter-cluster hydrogen bonding interactions play a key role in CO₂ capture in the CFA-1 analogue **1-OH** (Figure 3). CFA-1 contains crystallographically distinct, peripheral metal sites (Zn_A and Zn_E), and the distance between the Zn_E centers of neighboring metal nodes (~7.7 Å) enables the formation of a hydrogen-bonded bicarbonate dimer upon CO₂ adsorption. Such metal-based, synergistic binding mechanisms are rare in MOFs since metal sites/clusters are usually separated by relatively large distances.

While PXLE is gaining attention, it remains less explored than other PSM methods. When available at a MOF metal node, X-type ligands offer a handle for precise placement of ligand-based functional groups and greater stability against volatilization than dative PSM approaches. The combined reactivity of the framework metal and X-type ligand can also be exploited to generate highly reactive species or enable metal–ligand cooperativity for selective gas adsorption processes or new catalytic applications.^{104–106} Herein we show that the Zn–OH groups in **1-OH** act as strong Brønsted bases and undergo PXLE with a range of substrates containing mildly acidic E–H (E = C, N, O) bonds. The reaction of **1-OH** with aniline (PhNH₂) results in the formation of Zn–NHPh species, and CO₂ adsorption measurements for the resulting MOFs, **1-NHPh_x** (x = 0.9, 2.5), show steep, low-pressure uptake exceeding that of the parent **1-OH**. In situ diffuse-reflectance infrared Fourier transform spectroscopy (DRIFTS) experiments reveal that the Zn–NHPh groups in **1-NHPh_x** react with CO₂ to generate zinc carbamate (Zn–O₂CNHPh) species that have a higher CO₂ affinity than the parent Zn–

OH groups. CO₂ adsorption and DRIFTS studies with an anilide-exchanged analogue of MFU-4l (**2-NHPh**) further support the enhanced reactivity of the Zn–NHPh groups.

RESULTS AND DISCUSSION

The ligand-exchanged MOFs **1-E** were generated by treating **1-OH** with an excess (~5 equiv per Zn–OH group) of acidic E–H (E = C, N, O) substrates in a dichloromethane or 1,4-dioxane solution (Table 1). **1-NHPh**_{0.9} was prepared similarly

Table 1. Products (1-E) of Brønsted Acid–Base PXLE Reactions

1-E	formula	BET surface area (m ² g ⁻¹)	pK _a (DMSO) ^a	
			H-E	
1-OH	Zn ₅ (OH) ₄ (bibta) ₃	2326		
1-CH₂NO₂ ^c	Zn ₅ (CH ₂ NO ₂) ₄ (bibta) ₃	2013	H-CH ₂ NO ₂	17.2 ✓
1-OPh ^b	Zn ₅ (OPh) ₄ (bibta) ₃	1443	H-OPh	18.0 ✓
1-CCPh ^c	Zn ₅ (CCPh) ₄ (bibta) ₃	1470	H-CCPh	28.8 ✓
1-NHPh _{2.5} ^b	Zn ₅ (NHPh) _{2.5} (OH) _{1.5} (bibta) ₃	2005	H-NHPh	30.6 ✓
1-NHPh _{0.9} ^b	Zn ₅ (NHPh) _{0.9} (OH) _{3.1} (bibta) ₃	2070	H-CH ₂ CN	31.3 ✗

^apK_a values of the substrates in DMSO.^{111,112} ^b¹H NMR spectroscopy was used to establish the empirical formula. ^cIR spectroscopy was used to establish the empirical formula.

using 0.25 equiv of aniline per Zn–OH group. The Brønsted acid–base reactions result in PXLE at the Zn–OH sites with concomitant formation of H₂O. Powder X-ray diffraction (PXRD) patterns of the products indicate that no major structural changes occur as a result of the postsynthetic reactions (Figure S1). Acid-digested ¹H NMR spectra were used to quantify the extent of PXLE in **1-OPh**, **1-NHPh**_{0.9}, and **1-NHPh**_{2.5}. Integration of the spectrum measured for **1-OPh** gives a H₂bibta/PhOH ratio of 1:1.3, confirming that phenoxide is exchanged at all four peripheral Zn–OH sites of the metal nodes (Figure S11). The spectra of **1-NHPh**_{0.9} and **1-NHPh**_{2.5} show H₂bibta/PhNH₂ ratios of 1:0.3 and 1:0.82, indicating that the PXLE reactions incorporate ~0.9 and ~2.5 anilide groups per cluster (Figures S12 and S13). Despite numerous attempts to digest **1-CH₂NO₂** and **1-CCPh** under different conditions, ¹H NMR spectra suitable for quantifying the ligand exchange could not be obtained owing to acid-induced side reactions (Figures S15 and S16). However, the DRIFT spectra of **1-CH₂NO₂**, **1-CCPh**, and **1-OPh** show nearly complete disappearance of the ν(O–H) bands corresponding to the Zn–OH groups, supporting quantitative ligand exchange (Figures 4 and S6–S8). The DRIFT spectrum of **1-CH₂NO₂** also contains a band at 1600 cm⁻¹ assigned as the ν(C=N) mode of the nitromethanate ligand. The frequency of this band is consistent with significant C=N double-bond character and similar to that reported for κ²-O,O-nitromethanate complexes.^{107–109} The DRIFT spectrum of **1-OPh** shows new bands corresponding to ν(C–H) modes of the phenoxide group at 2989 and 3010 cm⁻¹, ν(C=C) modes at 1591 and 1491 cm⁻¹, and a C–O stretch at 1291 cm⁻¹. **1-CCPh** exhibits a ν(C≡C) band at 2119 cm⁻¹ that is in good agreement with those observed for related zinc

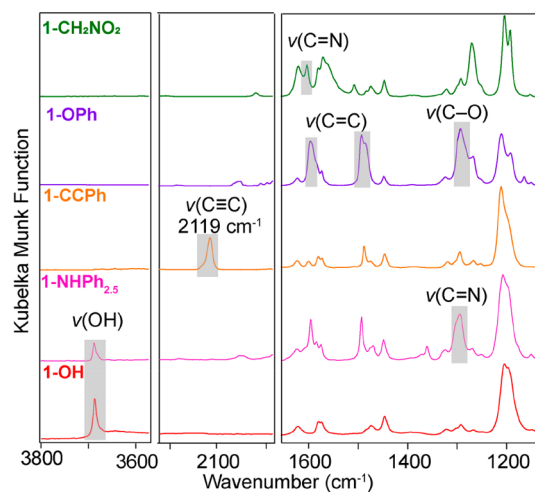


Figure 4. DRIFTS spectra of **1-CH₂NO₂**, **1-OPh**, **1-CCPh**, **1-NHPh**_{2.5}, and **1-OH**.

acetylide species generated at the metal nodes of MFU-4l.¹⁰⁰ The ν(O–H) band arising from the Zn–OH groups remains present in the DRIFT spectra of **1-NHPh**_{0.9} and **1-NHPh**_{2.5}, albeit with lower relative intensity compared to **1-OH**. This observation is consistent with the incomplete incorporation of Zn–NHPh groups, as determined from the acid-digested ¹H NMR spectra. The DRIFT spectra also contain ν(C=N) and ν(N–H) bands attributable to the anilide group at 1292 and 3391 cm⁻¹, respectively. The presence of a single ν(N–H) band supports N–H bond activation and the formation of a metal anilide species rather than coordination of the neutral amine. In the latter case, two ν(N–H) bands would be expected in the IR spectrum.¹¹⁰

The ¹H NMR and DRIFT spectra obtained after treating **1-OH** with neat acetonitrile [pK_a(DMSO) = 31.3] show no evidence of a PXLE reaction to form zinc cyanomethide species (Figures S10 and S17). This observation reveals the upper limit of the basicity of the Zn–OH groups in **1-OH**, which falls just short of the pK_a(DMSO) value of 32 for H₂O. Metal aqua complexes are typically more acidic than uncoordinated H₂O, but the magnitude of the decrease in pK_a is strongly influenced by the metal identity, coordination environment, and charge.¹¹³ In fact, molecular complexes with terminal M–OH (M = Ni, Cu, Au) groups are well-known to activate weakly acidic C–H bonds with pK_a(DMSO) values greater than 30.^{114–119} In the present case, the strong Lewis acidity of Zn²⁺, which would normally lead to less basic Zn–OH groups, may be counteracted by the strong benzotriazolate donor ligands and MOF microenvironment. Indeed, Gascon and co-workers found that MOF-immobilized aniline groups exhibit enhanced basicity compared to the homogeneous molecular analogue.¹²⁰ Consequently, the Brønsted acid–base PXLE reactions shown here for **1-OH** represent the first examples of activation of weakly acidic E–H functional groups by terminal Zn–OH species.

Samples of **1-E** were desolvated by heating at 100 °C under vacuum. The Brunauer–Emmett–Teller (BET) surface areas calculated from N₂ adsorption isotherms are all lower than that of **1-OH**, consistent with the incorporation of larger X-type ligands (Table 1 and Figures S3 and S4). CO₂ adsorption isotherms measured at 300 K for **1-CH₂NO₂**, **1-OPh**, and **1-CCPh** show linear adsorption profiles indicative of only weak physisorptive interactions (Figure S18). On the other hand, **1-**

NHPh_{0.9} and 1-NHPh_{2.5} exhibit steep, low-pressure CO₂ uptake similar to that of 1-OH (Figures 5 and S19). The

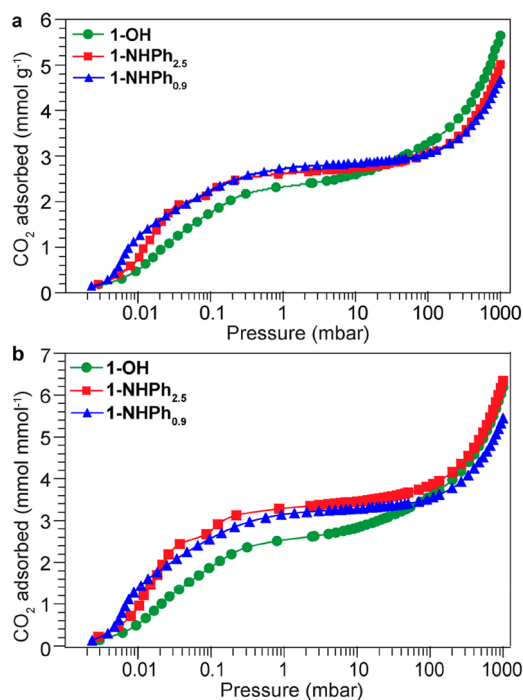


Figure 5. Semilogarithmic plots of CO₂ adsorption isotherms (300 K) measured for 1-OH, 1-NHPh_{2.5}, and 1-NHPh_{0.9} plotted in terms of (a) mmol of CO₂ per g of MOF and (b) mmol of CO₂ per mmol of MOF.

isotherms for the anilide-functionalized MOFs are distinctly steeper in the low-pressure region with slightly higher gravimetric capacities up to 10 mbar of CO₂. Because the PhNH⁻/OH⁻ ligand exchange results in a considerable

increase in the molecular weights of 1-NHPh_{0.9} and 1-NHPh_{2.5}, plotting the CO₂ uptake on a per formula unit basis (mmol of CO₂ per mmol of MOF) better highlights the differences. At 1 mbar, 1-NHPh_{0.9} and 1-NHPh_{2.5} adsorb 3.18 and 3.31 mmol mmol⁻¹ of CO₂, respectively, which are considerably higher than the 2.58 mmol mmol⁻¹ adsorbed by 1-OH. The theoretical density of Zn–X (X = OH, NHPh) groups in the MOFs is 4 mmol mmol⁻¹, meaning that the chemisorption sites reach saturation beyond 100 mbar of CO₂ pressure. The enhanced low-pressure CO₂ adsorption in 1-NHPh_{0.9} and 1-NHPh_{2.5} should arise from a greater thermodynamic driving force for reaction of the Zn–NHPh groups with CO₂ to form Zn–O₂CNHPh species compared to the Zn–OH + CO₂ ⇌ Zn–O₂COH chemisorption reaction. Unfortunately, attempts to measure variable-temperature isotherms for 1-NHPh_{0.9} and 1-NHPh_{2.5} and calculate isosteric heats of adsorption have been hindered by their poor thermal stability. Repeated thermal activation leads to a gradual decline in the CO₂ capacity and crystallinity (Figures S20 and S21). Consequently, DFT calculations have been carried out on model Kuratowski clusters to gain insight into the relative CO₂ binding energies of Zn–NHPh and Zn–OH groups (see the Supporting Information for details). Indeed, the CO₂ binding energy calculated for the formation of Zn–O₂CNHPh species (82.90 kJ mol⁻¹) is found to be considerably greater than that for the Zn–O₂COH groups (47.48 kJ mol⁻¹).

Variable-temperature DRIFTS experiments have been used to gain further insight into the reaction of 1-NHPh_{0.9} and 1-NHPh_{2.5} with CO₂ (Figure 6). At room temperature, the CO₂-loaded MOFs 1-NHPh_{0.9}-CO₂ and 1-NHPh_{2.5}-CO₂ exhibit IR bands at 2650, 1584, 1500, and 1342 cm⁻¹ that match those of the hydrogen-bonded Zn_E-HCO₃ species in 1-OH (Figure 3).⁹⁵ Accordingly, the presence of these bands indicates that pairs of Zn–OH groups remain at the Zn_E sites of the anilide-exchanged MOFs. In addition, weak bands appear at 1414 and 1664 cm⁻¹ in the DRIFT spectrum of 1-NHPh_{0.9}-CO₂ under a

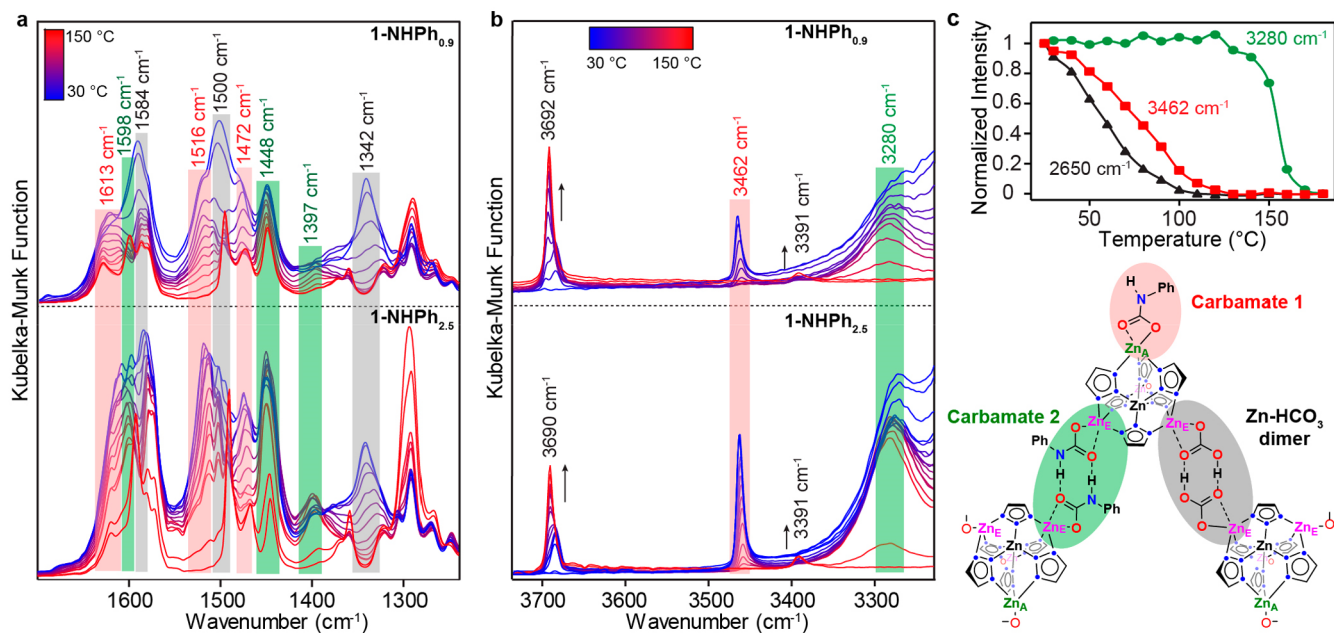


Figure 6. (a and b) Evolution of the DRIFT spectra of 1-NHPh_{0.9}-CO₂ and 1-NHPh_{2.5}-CO₂ upon heating under a N₂ atmosphere. The highlighted regions are bands corresponding to Zn_E-HCO₃ (gray), Carbamate 1 (red), and Carbamate 2 (green) species. (c) Temperature-dependent evolution of selected IR bands in 1-NHPh_{2.5}-CO₂.

CO₂ atmosphere but quickly vanish when the sample is placed under flowing N₂ (Figure S28). These bands are nearly identical in frequency and behavior with those observed for the Zn_A-O₂COH sites in **1-OH**, which are isolated and unable to engage in intercluster hydrogen-bonding interactions (Figure S27). However, they are absent in the spectrum of **1-NHPh**_{2.5}-CO₂ measured under CO₂, indicating complete PhNH⁻/OH⁻ exchange at the Zn_A sites of this material (Figure S29). Further inspection of the DRIFT spectra reveals a new set of bands at 1613 and 1472 cm⁻¹ that can be assigned as asymmetric and symmetric ν(C-O) modes of a distinct Zn-O₂CNHPh species (Carbamate 1). This species also gives rise to a carbamate ν(C-N) + δ(N-H) (amide II) mode at 1516 cm⁻¹ and a sharp ν(N-H) band at 3462 cm⁻¹. The latter is blue-shifted by 71 cm⁻¹ compared to the ν(N-H) band found in **1-NHPh**_{2.5} (3391 cm⁻¹). Insertion of CO₂ into the metal amide bonds of small-molecule complexes to form metal carbamates has been shown to result in a similarly blue-shifted ν(N-H) band.¹²¹ The DRIFT spectrum of **1-NHPh**_{2.5}-CO₂ clearly shows the presence of at least one additional Zn-O₂CNHPh species (Carbamate 2) characterized by a pair of asymmetric and symmetric ν(C-O) bands at 1598 and 1448 cm⁻¹ and a broad ν(N-H) band at 3280 cm⁻¹. The IR bands assigned to Carbamate 2 also appear in the DRIFT spectrum of **1-NHPh**_{0.9}-CO₂ but with lower relative intensity.

The presence of the distinct Carbamate 1 and Carbamate 2 species is supported by the evolution of the corresponding DRIFTS bands upon heating the CO₂-loaded MOFs to 150 °C under a N₂ flow. The most striking observation in the variable-temperature spectra is the difference in the rates of disappearance of the carbamate ν(N-H) bands at 3462 and 3280 cm⁻¹ (Figure 6c). In the spectrum of **1-NHPh**_{2.5}-CO₂, the former almost completely devolves before the onset of the disappearance of the band at 3280 cm⁻¹. This behavior clearly indicates that Carbamate 2 exhibits much stronger CO₂ binding than Carbamate 1. The same trend is observed for the bands corresponding to Carbamate 1 and Carbamate 2 in the 1200–1700 cm⁻¹ range, but the overlap in this region makes them more difficult to discern. At the same time, the features associated with the hydrogen-bonded Zn-HCO₃ species appear to devolve in the lower-temperature regime with Carbamate 1.

The relatively weak CO₂ binding and sharp, blue-shifted ν(N-H) band (3462 cm⁻¹) observed for Carbamate 1 elicit its association with isolated Zn_A-O₂CNHPh sites. This assignment is further supported by a comparison with an anilide-functionalized MFU-4l analogue (vide infra). Accordingly, the broad ν(N-H) band of Carbamate 2 (3280 cm⁻¹) and its greater CO₂ affinity are consistent with intercluster hydrogen-bonding interactions resembling those at the Zn_E-OH sites in **1-OH**. A similar broadening and red-shifting of the ν(N-H) bands has been observed for hydrogen-bonded alkyl carbamate dimers.¹²² However, the situation at the Zn_E sites is obfuscated by the three possible ligand combinations within each pocket (Figure S33). The DRIFTS data clearly show that some fraction of sites are occupied by Zn_E-OH pairs that result in hydrogen-bonded Zn_E-O₂COH⋯HOCO₂-Zn_E species. The remaining pockets should contain Zn_E-NHPh with neighboring Zn_E-OH or Zn_E-NHPh groups. Statistically, the high anilide loading in **1-NHPh**_{2.5} and observation of Zn_E-O₂COH⋯HOCO₂-Zn_E species necessitates the presence of Zn_E-NHPh⋯PhNHCO₂-Zn_E pairs. However, a slightly red-shifted, residual ν(O-H) band at 3280 cm⁻¹ in the DRIFT

spectrum of **1-NHPh**_{2.5}-CO₂ signals the presence of unreacted Zn-OH groups, which may arise from the formation of unsymmetrical Zn_E-O₂CNHPh⋯HO-Zn_E pairs. Consequently, while the assignment of the Carbamate 2 species to the Zn_E sites is well-founded, the identity of the hydrogen-bond partner remains ambiguous. Nevertheless, the variable-temperature DRIFTS data clearly show enhanced CO₂ binding at both the Zn_A-NHPh and Zn_E-NHPh sites. While the Zn_A-O₂COH groups in the parent **1-OH** readily desorb CO₂ at room temperature, the Zn_A-O₂CNHPh species only devolve upon heating. Similarly, the hydrogen-bonded Zn_E-O₂CNHPh species are much more robust than the Zn_E-O₂COH congeners and remain intact until nearly 150 °C.

To further probe the effect of Zn-NHPh groups on CO₂ adsorption and support the assignments above, an anilide-functionalized MFU-4l analogue, **2-NHPh**, was synthesized using the same PXLE procedure as that employed for **1-NHPh**_{2.5}. MFU-4l contains Kuratowski-type metal nodes, but the Zn-X sites are crystallographically equivalent without the possibility of intercluster hydrogen-bonding interactions between bicarbonate ligands (Figure 2). As a result, **2-OH** exhibits a lower CO₂ capacity and affinity than **1-OH**.⁹⁷ The PXRD pattern of **2-NHPh** matches that of parent MOF, and the acid-digested ¹H NMR spectrum shows a H₂btdd/PhNH₂ ratio of 1:0.63, indicating the incorporation of ~1.9 anilide groups per cluster. The N₂ adsorption isotherm measured for **2-NHPh** gave a calculated BET surface area of 2816 m² g⁻¹, which is lower than that of the parent MFU-4l (3770 m² g⁻¹) but consistent with the presence of the larger anilide ligands (Figure S5). CO₂ adsorption isotherms (300 K) show that **2-NHPh** adsorbs a greater amount of CO₂ than **2-OH** along the entire pressure range up to 1 bar (Figure 7a), with an adsorption capacity of 0.95 mmol g⁻¹ at 1 mbar. Notably, **2-NHPh** displays better thermal stability than the **1-NHPh**_x derivatives, and only a small decrease in the CO₂ capacity was observed after several adsorption-activation cycles (Figure S22). Consequently, variable-temperature CO₂ isotherms have been used to calculate the isosteric heat of adsorption (Q_{st}) as a function of CO₂ loading (Figure S26). The observed maximum of 65 kJ mol⁻¹ reflects a strong chemisorption mechanism but is only slightly higher than the value previously reported for **2-OH** (63 kJ mol⁻¹).⁹⁷

The isolated Zn-O₂CNHPh species formed in **2-NHPh**-CO₂ should be expected to exhibit an IR spectroscopic signature similar to that of Zn_A-O₂CNHPh groups in **1-NHPh**-CO₂. This is indeed the case, and **2-NHPh**-CO₂ gives rise to a single set of new carbamate bands at 1442, 1513, 1606, and 3464 cm⁻¹ that closely match those observed for **1-NHPh**_x-CO₂ (Figures 7b and S31). Consistent with our previous findings, the Zn-OH groups remaining in **2-NHPh** exhibit weak CO₂ binding, and bands assigned to the corresponding Zn-HCO₃ species at 1661, 1425, and 1207 cm⁻¹ quickly disappear when the atmosphere in the sample chamber is switched from CO₂ to flowing N₂.⁹⁷ However, the IR spectral features corresponding to the Zn-O₂CNHPh groups are stable under a N₂ atmosphere and only begin to devolve upon heating (Figure S31).

CONCLUSIONS

The Zn-OH groups in **1-OH** are unexpectedly strong bases capable of activating E-H functional groups with pK_a(DMSO) values approaching 30. The resulting Brønsted acid-base PXLE reactions offer an efficient and robust method for

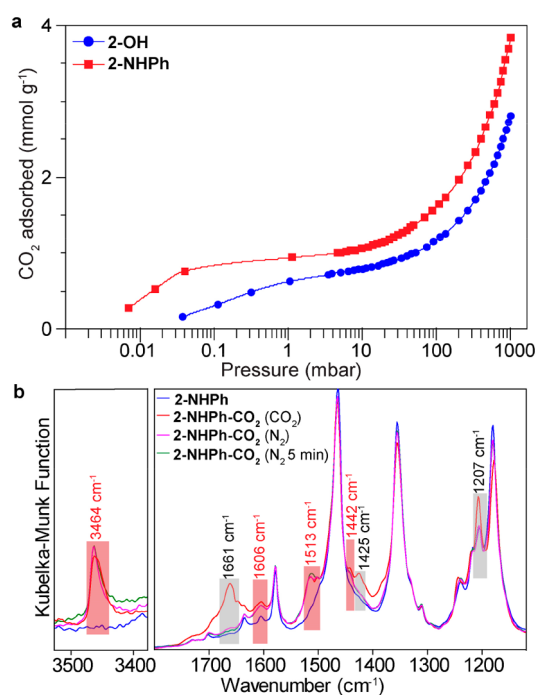


Figure 7. (a) Semilogarithmic plots of CO₂ adsorption isotherms (300 K) measured for 2-NHPh and 2-OH. (b) Room temperature DRIFT spectra measured for 2-NHPh after exposure to CO₂ and subsequent purging with N₂. The bands highlighted in gray and red are associated with Zn-HCO₃ and Zn-O₂CNHPh species, respectively.

functionalizing Kuratowski-type metal nodes with X-type ligands that modulate gas adsorption or catalytic properties. CO₂ adsorption studies with 1-NHPh_{0.9} and 1-NHPh_{2.5} demonstrate the utility of this approach, and the partial incorporation of Zn-NHPh groups increases low-pressure CO₂ uptake in comparison to the parent 1-OH. In situ DRIFTS experiments reveal that CO₂ reacts with the Zn-NHPh groups to form two distinct zinc carbamate species, both of which exhibit greater CO₂ affinities than their Zn-OH congeners. The Brønsted acid–base PXLE method described here for 1-OH resembles SALI developed for Zr-based MOFs.⁶⁴ However, the ability to apply both PSME and PXLE in MOFs containing Kuratowski-type nodes presents unique opportunities to exploit metal-based reactivity and design metal–ligand cooperativity.

EXPERIMENTAL SECTION

General Considerations. 1-OH and 2-OH were synthesized according to reported procedures.^{95,97} Nitromethane (Acros Organic, 99+%), aniline (Mallinckrodt, ACS grade), and phenylacetylene (Alfa Aesar, 98+) were dried over CaH₂, distilled, and stored in a N₂-filled glovebox. Phenol (Alfa Aesar, 99+) was used as received. Tetrahydrofuran, 1,4-dioxane, acetonitrile, and dichloromethane were degassed by sparging with ultrahigh-purity argon and dried via passage through columns of drying agents using a solvent purification system from Pure Process Technologies. All other solvents and reagents were purchased from commercial suppliers and used as received. Routine powder X-ray diffraction patterns for phase identification were collected on a Rigaku Miniflex 600 diffractometer using nickel-filtered Cu K α radiation ($\lambda = 1.5418 \text{ \AA}$). Elemental microanalyses were performed by Robertson Microлит Laboratories, Ledgewood, NJ. Solution-state NMR spectra were measured using a Bruker DPX 400 MHz spectrometer. ¹H NMR spectra were collected using 180° water-selective excitation sculpting with default parameters

and pulse shapes.¹²³ Briefly, spectra were collected using selective pulses of 1 ms with the transmitter frequency set to the center of the solvent resonance. The recycle delay between scans was 2 s, 16K points were collected, and the acquisition time was 0.7 s. For ¹H NMR spectra, the solvent resonance was referenced as an internal standard. Samples were digested for solution-state ¹H NMR analysis by suspending ~10 mg of solid in CF₃CO₂H (0.5 mL) or H₂SO₄ (1–3 drops) and gently heating the suspensions until all of the solids dissolved. Deuterated dimethyl sulfoxide (DMSO-*d*₆; 0.1–1 mL) was then added to provide a lock signal for shimming.

Gas Adsorption Isotherms. Single-component gas adsorption isotherms were measured using a Micromeritics 3Flex surface characterization analyzer. All measurements were performed using ultrahigh purity grade gases (99.999%) purchased from Praxair (N₂, NI 5.0UH-K; CO₂, CD 5.0LS-K). Prior to analysis, samples (100–200 mg) were transferred to oven-dried and tared sample tubes equipped with TranSeals (Micromeritics) and heated to 100 or 150 °C (1 °C min⁻¹) under vacuum until the outgas rate was less than 0.0033 mbar min⁻¹. BET surface areas were calculated from the N₂ adsorption isotherms (77 K) by fitting the data to the BET equation, with the appropriate pressure range ($0.0001 \leq P/P_0 \leq 0.1$) determined by the consistency criteria of Rouquerol.¹²⁴ A Micromeritics thermocouple-controlled heating mantle was used to maintain the sample temperature for isotherms measured between 300 and 373 K.

DRIFTS Measurements. DRIFT spectra were recorded using a Bruker Tensor spectrometer equipped with a liquid N₂-cooled MCT detector and a Praying Mantis diffuse-reflectance accessory (Harrick Scientific). Background spectra were collected with anhydrous KBr. Samples were diluted with anhydrous KBr and loaded into the sample cup of a high-temperature reaction chamber fitted with KBr windows. The chamber was sealed and placed under a flow of dry N₂ gas. Variable-temperature DRIFT spectra were measured periodically, while heating the samples from 25 to 150 °C. For in situ CO₂ adsorption experiments, the chamber was sealed, placed under a flow of N₂ gas, and heated from 28 to 150 °C while the DRIFT spectra were monitored to confirm activation. Upon cooling, the sample flow gas was switched to pure CO₂ using a three-way valve, and DRIFT spectra were recorded until the sample reached equilibrium. The sample flow gas was then switched back to N₂, and DRIFT spectra were measured periodically while the sample was heated from 28 to 150 °C.

Synthesis of 1-CH₂NO₂. In a N₂-filled glovebox, a 20 mL scintillation vial was charged with 1-OH (0.176 g, 0.64 mmol of Zn-OH) and a 0.5 M solution of nitromethane (6.4 mL, 3.2 mmol) in dichloromethane. The suspension was kept at room temperature for 72 h. The solution was decanted, and the MOF was washed with 3 × 20 mL of dichloromethane. Elem anal. Calcd for Zn₃(CH₂NO₂)₄(bibta)₃ (Zn₃C₄₀H₂₆N₂₂O₈): C, 37.84; H, 2.06; N, 24.27. Found: C, 37.72; H, 2.20; N, 23.60.

Synthesis of 1-OPh. In a N₂-filled glovebox, a 20 mL scintillation vial was charged with 1-OH (0.0925 g, 0.34 mmol of Zn-OH) and a 0.5 M solution of phenol (3.4 mL, 1.7 mmol) in 1,4-dioxane. The suspension was kept at room temperature for 72 h. The solution was decanted, and the MOF was washed with 3 × 20 mL of dioxanes. Elem anal. Calcd for Zn₅(OPh)₄(bibta)₃·2H₂O (Zn₅C₆₀H₄₂N₁₈O₆): C, 50.11; H, 2.94; N, 17.53. Found: C, 49.43; H, 2.46; N, 17.69.

Synthesis of 1-PhCCH. In a N₂-filled glovebox, a 20 mL scintillation vial was charged with 1-OH (0.1503 g, 0.54 mmol of Zn-OH) and a 0.5 M solution of phenylacetylene (5.5 mL, 2.7 mmol) in 1,4-dioxane. The suspension was kept at room temperature for 16 h. The solution was decanted, and the MOF was washed with 3 × 20 mL of dioxanes. Elem anal. Calcd for Zn₅(CCPh)₄(bibta)₃·5H₂O (Zn₅C₆₈H₄₈N₁₈O₅): C, 53.58; H, 3.17; N, 16.54. Found: C, 53.05; H, 2.37; N, 17.46.

Synthesis of 1-NHPh_{2.5}. In a N₂-filled glovebox, a 20 mL scintillation vial was charged with 1-OH (0.1165 g, 0.42 mmol of Zn-OH) and a 0.5 M solution of aniline (4.2 mL, 2.1 mmol) in 1,4-dioxane, resulting in a rapid color change of the solid from beige to yellow. The suspension was kept at room temperature for 72 h. The

solution was decanted, and the MOF was washed with 3×20 mL of 1,4-dioxane. Elem. anal. Calcd for $\text{Zn}_3(\text{NHPH})_{2.5}(\text{OH})_{1.5}(\text{bibta})_3 \cdot 4\text{H}_2\text{O}$ ($\text{Zn}_3\text{C}_{51}\text{H}_{42.5}\text{N}_{20.5}\text{O}_{5.5}$): C, 45.12; H, 3.16; N, 21.15. Found: C, 44.05; H, 2.50; N, 21.59.

Synthesis of 1-NHPH_{0.9}. In a N_2 -filled glovebox, a 20 mL scintillation vial was charged with 1-OH (0.120 g, 0.44 mmol of Zn-OH) and 1,4-dioxane (5 mL). A 0.1 M solution of aniline (1.1 mL, 0.11 mmol) in 1,4-dioxane was added, resulting in a rapid color change of the solid from beige to yellow. The suspension was kept at room temperature for 24 h. The solution was decanted, and the MOF was washed with 3×20 mL of 1,4-dioxane. A light-yellow solid was collected by filtration. The solution-state ^1H NMR spectrum of an acid-digested sample shows a $\sim 3:0.9$ ratio of $\text{H}_2(\text{bibta})/\text{PhNH}_2$, which is consistent with an empirical formula of $\text{Zn}(\text{ZnOH})_{3.1}(\text{ZnNHPH})_{0.9}(\text{bibta})_3$.

Synthesis of 2-NHPH. In a N_2 -filled glovebox, a 20 mL scintillation vial was charged with 2-OH (0.0760 g, 0.26 mmol of Zn-OH) and a 0.5 M solution of aniline (2.6 mL, 1.3 mmol) in 1,4-dioxane. The suspension was kept at room temperature for 72 h. The solution was decanted, and the MOF was washed with 3×20 mL of 1,4-dioxane. The solution-state ^1H NMR spectrum of an acid-digested sample shows a $\sim 3:1.9$ ratio of $\text{H}_2(\text{btdd})/\text{PhNH}_2$, which is consistent with an empirical formula of $\text{Zn}(\text{ZnOH})_{2.1}(\text{ZnNHPH})_{1.9}(\text{btdd})_3$.

■ ASSOCIATED CONTENT

Supporting Information

The Supporting Information is available free of charge at <https://pubs.acs.org/doi/10.1021/acs.inorgchem.1c01077>.

Analytical data, attenuated-total-reflectance IR and NMR spectra, gas sorption isotherms and data, and DFT computational details and results (PDF)

■ AUTHOR INFORMATION

Corresponding Author

Casey R. Wade – Department of Chemistry and Biochemistry, The Ohio State University, Columbus, Ohio 43210, United States; orcid.org/0000-0002-7044-9749; Email: wade.521@osu.edu

Authors

Caitlin E. Bien – Department of Chemistry and Biochemistry, The Ohio State University, Columbus, Ohio 43210, United States

Zhongzheng Cai – Department of Chemistry and Biochemistry, The Ohio State University, Columbus, Ohio 43210, United States

Complete contact information is available at: <https://pubs.acs.org/doi/10.1021/acs.inorgchem.1c01077>

Author Contributions

[†]These authors contributed equally to this work.

Notes

The authors declare no competing financial interest.

■ ACKNOWLEDGMENTS

This work was supported by an Early Career Faculty grant (Grant 80NSSC18K1504) from NASA's Space Technology Research Grants Program and The Ohio State University Materials Research Seed Grant Program, funded by the Center for Emergent Materials (Grants NSF-MRSEC and DMR-1420451) and the Institute for Materials Research. The authors also thank the Ohio Supercomputer Center for computational resources.¹²⁵

■ REFERENCES

- (1) Zhou, H.-C.; Long, J. R.; Yaghi, O. M. Introduction to Metal-Organic Frameworks. *Chem. Rev.* **2012**, *112*, 673–674.
- (2) Chen, Z.; Wasson, M. C.; Drout, R. J.; Robison, L.; Idrees, K. B.; Knapp, J. G.; Son, F. A.; Zhang, X.; Hierse, W.; Kühn, C.; Marx, S.; Hernandez, B.; Farha, O. K. The State of the Field: From Inception to Commercialization of Metal-Organic Frameworks. *Faraday Discuss.* **2021**, *225*, 9–69.
- (3) Yu, J.; Xie, L.-H.; Li, J.-R.; Ma, Y.; Seminario, J. M.; Balbuena, P. B. CO₂ Capture and Separations Using MOFs: Computational and Experimental Studies. *Chem. Rev.* **2017**, *117*, 9674–9754.
- (4) Cui, W.; Hu, T.; Bu, X. Metal-Organic Framework Materials for the Separation and Purification of Light Hydrocarbons. *Adv. Mater.* **2020**, *32*, 1806445.
- (5) Li, H.; Li, L.; Lin, R.-B.; Zhou, W.; Zhang, Z.; Xiang, S.; Chen, B. Porous Metal-Organic Frameworks for Gas Storage and Separation: Status and Challenges. *EnergyChem.* **2019**, *1*, 100006.
- (6) Lin, R.-B.; Xiang, S.; Zhou, W.; Chen, B. Microporous Metal-Organic Framework Materials for Gas Separation. *Chem.* **2020**, *6*, 337–363.
- (7) Wang, Q.; Astruc, D. State of the Art and Prospects in Metal-Organic Framework (MOF)-Based and MOF-Derived Nanocatalysis. *Chem. Rev.* **2020**, *120*, 1438–1511.
- (8) Wei, Y.-S.; Zhang, M.; Zou, R.; Xu, Q. Metal-Organic Framework-Based Catalysts with Single Metal Sites. *Chem. Rev.* **2020**, *120*, 12089–12174.
- (9) Bavykina, A.; Kolobov, N.; Khan, I. S.; Bau, J. A.; Ramirez, A.; Gascon, J. Metal-Organic Frameworks in Heterogeneous Catalysis: Recent Progress, New Trends, and Future Perspectives. *Chem. Rev.* **2020**, *120*, 8468–8535.
- (10) Cai, W.; Wang, J.; Chu, C.; Chen, W.; Wu, C.; Liu, G. Metal-Organic Framework-Based Stimuli-Responsive Systems for Drug Delivery. *Adv. Sci.* **2019**, *6*, 1801526.
- (11) Baumann, A. E.; Burns, D. A.; Liu, B.; Thoi, V. S. Metal-Organic Framework Functionalization and Design Strategies for Advanced Electrochemical Energy Storage Devices. *Commun. Chem.* **2019**, *2*, 86.
- (12) Xie, L. S.; Skorupskii, G.; Dincă, M. Electrically Conductive Metal-Organic Frameworks. *Chem. Rev.* **2020**, *120*, 8536–8580.
- (13) Dang, D.; Wu, P.; He, C.; Xie, Z.; Duan, C. Homochiral Metal-Organic Frameworks for Heterogeneous Asymmetric Catalysis. *J. Am. Chem. Soc.* **2010**, *132*, 14321–14323.
- (14) Fracaroli, A. M.; Siman, P.; Nagib, D. A.; Suzuki, M.; Furukawa, H.; Toste, F. D.; Yaghi, O. M. Seven Post-Synthetic Covalent Reactions in Tandem Leading to Enzyme-like Complexity within Metal-Organic Framework Crystals. *J. Am. Chem. Soc.* **2016**, *138*, 8352–8355.
- (15) Drake, T.; Ji, P.; Lin, W. Site Isolation in Metal-Organic Frameworks Enables Novel Transition Metal Catalysis. *Acc. Chem. Res.* **2018**, *51*, 2129–2138.
- (16) Jiao, L.; Wang, J.; Jiang, H.-L. Microenvironment Modulation in Metal-Organic Framework-Based Catalysis. *Accounts Mater. Res.* **2021**, *2*, 327.
- (17) Xiao, D. J.; Oktawiec, J.; Milner, P. J.; Long, J. R. Pore Environment Effects on Catalytic Cyclohexane Oxidation in Expanded Fe₂(Dobdc) Analogues. *J. Am. Chem. Soc.* **2016**, *138*, 14371–14379.
- (18) Yuan, S.; Chen, Y.-P.; Qin, J.-S.; Lu, W.; Zou, L.; Zhang, Q.; Wang, X.; Sun, X.; Zhou, H.-C. Linker Installation: Engineering Pore Environment with Precisely Placed Functionalities in Zirconium MOFs. *J. Am. Chem. Soc.* **2016**, *138*, 8912–8919.
- (19) Shi, W.; Cao, L.; Zhang, H.; Zhou, X.; An, B.; Lin, Z.; Dai, R.; Li, J.; Wang, C.; Lin, W. Surface Modification of Two-Dimensional Metal-Organic Layers Creates Biomimetic Catalytic Microenvironments for Selective Oxidation. *Angew. Chem., Int. Ed.* **2017**, *56*, 9704–9709.
- (20) Xia, Q.; Li, Z.; Tan, C.; Liu, Y.; Gong, W.; Cui, Y. Multivariate Metal-Organic Frameworks as Multifunctional Heterogeneous Asym-

metric Catalysts for Sequential Reactions. *J. Am. Chem. Soc.* **2017**, *139*, 8259–8266.

(21) Liu, L.; Zhou, T.-Y.; Telfer, S. G. Modulating the Performance of an Asymmetric Organocatalyst by Tuning Its Spatial Environment in a Metal-Organic Framework. *J. Am. Chem. Soc.* **2017**, *139*, 13936–13943.

(22) Zhou, T.-Y.; Auer, B.; Lee, S. J.; Telfer, S. G. Catalysts Confined in Programmed Framework Pores Enable New Transformations and Tune Reaction Efficiency and Selectivity. *J. Am. Chem. Soc.* **2019**, *141*, 1577–1582.

(23) Grigoropoulos, A.; McKay, A. I.; Katsoulidis, A. P.; Davies, R. P.; Haynes, A.; Brammer, L.; Xiao, J.; Weller, A. S.; Rosseinsky, M. J. Encapsulation of Crabtree's Catalyst in Sulfonated MIL-101(Cr): Enhancement of Stability and Selectivity between Competing Reaction Pathways by the MOF Chemical Microenvironment. *Angew. Chem., Int. Ed.* **2018**, *57*, 4532–4537.

(24) Cohen, S. M.; Zhang, Z.; Boissonault, J. A. Toward "MetalloMOFzymes": Metal-Organic Frameworks with Single-Site Metal Catalysts for Small-Molecule Transformations. *Inorg. Chem.* **2016**, *55*, 7281–7290.

(25) Cohen, S. M. Postsynthetic Methods for the Functionalization of Metal-Organic Frameworks. *Chem. Rev.* **2012**, *112*, 970–1000.

(26) Cohen, S. M. The Postsynthetic Renaissance in Porous Solids. *J. Am. Chem. Soc.* **2017**, *139*, 2855–2863.

(27) Yin, Z.; Wan, S.; Yang, J.; Kurmoo, M.; Zeng, M. H. Recent Advances in Post-Synthetic Modification of Metal-Organic Frameworks: New Types and Tandem Reactions. *Coord. Chem. Rev.* **2019**, *378*, 500–512.

(28) Kalaj, M.; Cohen, S. M. Postsynthetic Modification: An Enabling Technology for the Advancement of Metal-Organic Frameworks. *ACS Cent. Sci.* **2020**, *6*, 1046–1057.

(29) Mandal, S.; Natarajan, S.; Mani, P.; Pankajakshan, A. Post-Synthetic Modification of Metal-Organic Frameworks Toward Applications. *Adv. Funct. Mater.* **2021**, *31*, 2006291.

(30) Brozek, C. K.; Dinčá, M. Cation Exchange at the Secondary Building Units of Metal-Organic Frameworks. *Chem. Soc. Rev.* **2014**, *43*, 5456–5467.

(31) Ezazi, A. A.; Gao, W.-Y.; Powers, D. C. Leveraging Exchange Kinetics for the Synthesis of Atomically Precise Porous Catalysts. *ChemCatChem* **2021**, *13*, 2117–2131.

(32) Karagiari, O.; Bury, W.; Mondloch, J. E.; Hupp, J. T.; Farha, O. K. Solvent-Assisted Linker Exchange: An Alternative to the de Novo Synthesis of Unattainable Metal-Organic Frameworks. *Angew. Chem., Int. Ed.* **2014**, *53*, 4530–4540.

(33) Deria, P.; Mondloch, J. E.; Karagiari, O.; Bury, W.; Hupp, J. T.; Farha, O. K. Beyond Post-Synthesis Modification: Evolution of Metal-Organic Frameworks via Building Block Replacement. *Chem. Soc. Rev.* **2014**, *43*, 5896–5912.

(34) Wang, Z.; Cohen, S. M. Postsynthetic Covalent Modification of a Neutral Metal-Organic Framework. *J. Am. Chem. Soc.* **2007**, *129*, 12368–12369.

(35) The terms L-type and X-type refer to neutral and anionic two-electron donor ligands, respectively. See: Green, M. L. H.; Parkin, G. Application of the Covalent Bond Classification Method for the Teaching of Inorganic Chemistry. *J. Chem. Educ.* **2014**, *91*, 807–816.

(36) K k cam-Demir,  .; Goldman, A.; Esrafilı, L.; Gharib, M.; Morsali, A.; Weingart, O.; Janiak, C. Coordinatively Unsaturated Metal Sites (Open Metal Sites) in Metal-Organic Frameworks: Design and Applications. *Chem. Soc. Rev.* **2020**, *49*, 2751–2798.

(37) Chui, S. S. A Chemically Functionalizable Nanoporous Material [Cu₃(TMA)₂(H₂O)₃]N. *Science* **1999**, *283*, 1148–1150.

(38) Farha, O. K.; Mulfort, K. L.; Hupp, J. T. An Example of Node-Based Postassembly Elaboration of a Hydrogen-Sorbing, Metal-Organic Framework Material. *Inorg. Chem.* **2008**, *47*, 10223–10225.

(39) Ingleson, M. J.; Heck, R.; Gould, J. A.; Rosseinsky, M. J. Nitric Oxide Chemisorption in a Postsynthetically Modified Metal-Organic Framework. *Inorg. Chem.* **2009**, *48*, 9986–9988.

(40) Banerjee, M.; Das, S.; Yoon, M.; Choi, H. J.; Hyun, M. H.; Park, S. M.; Seo, G.; Kim, K. Postsynthetic Modification Switches an

Achiral Framework to Catalytically Active Homochiral Metal-Organic Porous Materials. *J. Am. Chem. Soc.* **2009**, *131*, 7524–7525.

(41) Gheorghie, A.; Strudwick, B.; Dawson, D. M.; Ashbrook, S. E.; Woutersen, S.; Dubbeldam, D.; Tanase, S. Synthesis of Chiral MOF-74 Frameworks by Post-Synthetic Modification by Using an Amino Acid. *Chem. - Eur. J.* **2020**, *26*, 13957–13965.

(42) Hwang, Y. K.; Hong, D.-Y.; Chang, J.-S.; Jung, S. H.; Seo, Y.-K.; Kim, J.; Vimont, A.; Daturi, M.; Serre, C.; F rey, G. Amine Grafting on Coordinatively Unsaturated Metal Centers of MOFs: Consequences for Catalysis and Metal Encapsulation. *Angew. Chem., Int. Ed.* **2008**, *47*, 4144–4148.

(43) Li, B.; Zhang, Y.; Ma, D.; Li, L.; Li, G.; Li, G.; Shi, Z.; Feng, S. A Strategy toward Constructing a Bifunctionalized MOF Catalyst: Post-Synthetic Modification of MOFs on Organic Ligands and Coordinatively Unsaturated Metal Sites. *Chem. Commun.* **2012**, *48*, 6151–6153.

(44) Demessence, A.; D'Alessandro, D. M.; Foo, M. L.; Long, J. R. Strong CO₂ Binding in a Water-Stable, Triazolate-Bridged Metal-Organic Framework Functionalized with Ethylenediamine. *J. Am. Chem. Soc.* **2009**, *131*, 8784–8786.

(45) McDonald, T. M.; Lee, W. R.; Mason, J. A.; Wiers, B. M.; Hong, C. S.; Long, J. R. Capture of Carbon Dioxide from Air and Flue Gas in the Alkylamine-Appended Metal-Organic Framework Mmen-Mg₂(Dobpdc). *J. Am. Chem. Soc.* **2012**, *134*, 7056–7065.

(46) Lee, W. R.; Hwang, S. Y.; Ryu, D. W.; Lim, K. S.; Han, S. S.; Moon, D.; Choi, J.; Hong, C. S. Diamine-Functionalized Metal-Organic Framework: Exceptionally High CO₂ Capacities from Ambient Air and Flue Gas, Ultrafast CO₂ Uptake Rate, and Adsorption Mechanism. *Energy Environ. Sci.* **2014**, *7*, 744–751.

(47) Darunte, L. A.; Oetomo, A. D.; Walton, K. S.; Sholl, D. S.; Jones, C. W. Direct Air Capture of CO₂ Using Amine Functionalized MIL-101(Cr). *ACS Sustainable Chem. Eng.* **2016**, *4*, 5761–5768.

(48) Li, H.; Wang, K.; Feng, D.; Chen, Y.-P.; Verdegaa, W.; Zhou, H.-C. Incorporation of Alkylamine into Metal-Organic Frameworks through a Br nsted Acid-Base Reaction for CO₂ Capture. *ChemSusChem* **2016**, *9*, 2832–2840.

(49) Liao, P.-Q.; Chen, X.-W.; Liu, S.-Y.; Li, X.-Y.; Xu, Y.-T.; Tang, M.; Rui, Z.; Ji, H.; Zhang, J.-P.; Chen, X.-M. Putting an Ultrahigh Concentration of Amine Groups into a Metal-Organic Framework for CO₂ Capture at Low Pressures. *Chem. Sci.* **2016**, *7*, 6528–6533.

(50) Didas, S. A.; Choi, S.; Chaikittisilp, W.; Jones, C. W. Amine-Oxide Hybrid Materials for CO₂ Capture from Ambient Air. *Acc. Chem. Res.* **2015**, *48*, 2680–2687.

(51) Lu, W.; Sculley, J. P.; Yuan, D.; Krishna, R.; Zhou, H.-C. Carbon Dioxide Capture from Air Using Amine-Grafted Porous Polymer Networks. *J. Phys. Chem. C* **2013**, *117*, 4057–4061.

(52) Kang, M.; Kang, D. W.; Hong, C. S. Post-Synthetic Diamine-Functionalization of MOF-74 Type Frameworks for Effective Carbon Dioxide Separation. *Dalton Trans.* **2019**, *48*, 2263–2270.

(53) McDonald, T. M.; Mason, J. A.; Kong, X.; Bloch, E. D.; Gygi, D.; Dani, A.; Crocell , V.; Giordanino, F.; Odoh, S. O.; Drisdell, W. S.; Vlaisavljevich, B.; Dzubak, A. L.; Poloni, R.; Schnell, S. K.; Planas, N.; Lee, K.; Pascal, T.; Wan, L. F.; Prendergast, D.; Neaton, J. B.; Smit, B.; Kortright, J. B.; Gagliardi, L.; Bordiga, S.; Reimer, J. A.; Long, J. R. Cooperative Insertion of CO₂ in Diamine-Appended Metal-Organic Frameworks. *Nature* **2015**, *519*, 303–308.

(54) Fei, H.; Rogow, D. L.; Oliver, S. R. J. Reversible Anion Exchange and Catalytic Properties of Two Cationic Metal-Organic Frameworks Based on Cu(I) and Ag(I). *J. Am. Chem. Soc.* **2010**, *132*, 7202–7209.

(55) Schoedel, A.; Wojtas, L.; Kelley, S. P.; Rogers, R. D.; Eddaoudi, M.; Zaworotko, M. J. Network Diversity through Decoration of Trigonal-Prismatic Nodes: Two-Step Crystal Engineering of Cationic Metal-Organic Materials. *Angew. Chem., Int. Ed.* **2011**, *50*, 11421–11424.

(56) Mao, C.; Kudla, R. A.; Zuo, F.; Zhao, X.; Mueller, L. J.; Bu, X.; Feng, P. Anion Stripping as a General Method to Create Cationic Porous Framework with Mobile Anions. *J. Am. Chem. Soc.* **2014**, *136*, 7579–7582.

- (57) Ma, J.-P.; Yu, Y.; Dong, Y.-B. Fluorene-Based Cu(II)-MOF: A Visual Colorimetric Anion Sensor and Separator Based on an Anion-Exchange Approach. *Chem. Commun.* **2012**, *48*, 2946–2948.
- (58) Chen, Y.-Q.; Li, G.-R.; Chang, Z.; Qu, Y.-K.; Zhang, Y.-H.; Bu, X.-H. A Cu(I) Metal-Organic Framework with 4-Fold Helical Channels for Sensing Anions. *Chem. Sci.* **2013**, *4*, 3678.
- (59) Zhao, X.; Mao, C.; Luong, K. T.; Lin, Q.; Zhai, Q.-G.; Feng, P.; Bu, X. Framework Cationization by Preemptive Coordination of Open Metal Sites for Anion-Exchange Encapsulation of Nucleotides and Coenzymes. *Angew. Chem., Int. Ed.* **2016**, *55*, 2768–2772.
- (60) Luo, T.-Y.; Liu, C.; Eliseeva, S. V.; Muldoon, P. F.; Petoud, S.; Rosi, N. L. Rare Earth Pcu Metal-Organic Framework Platform Based on RE₄(M₃-OH)₄(COO)₆²⁺ Clusters: Rational Design, Directed Synthesis, and Deliberate Tuning of Excitation Wavelengths. *J. Am. Chem. Soc.* **2017**, *139*, 9333–9340.
- (61) Park, H. D.; Dincă, M.; Román-Leshkov, Y. Continuous-Flow Production of Succinic Anhydrides via Catalytic β -Lactone Carbonylation by Co(CO)₄ C_{Cr}-MIL-101. *J. Am. Chem. Soc.* **2018**, *140*, 10669–10672.
- (62) Brunet, G.; Robeyns, K.; Huynh, R. P. S.; Lin, J.-B.; Collins, S. P.; Facey, G. A.; Shimizu, G. K. H.; Woo, T. K.; Murugesu, M. Design Strategy for the Controlled Generation of Cationic Frameworks and Ensuing Anion-Exchange Capabilities. *ACS Appl. Mater. Interfaces* **2019**, *11*, 3181–3188.
- (63) do Pim, W. D.; Mendonça, F. G.; Brunet, G.; Facey, G. A.; Chevallerier, F.; Bucher, C.; Baker, R. T.; Murugesu, M. Anion-Dependent Catalytic C-C Bond Cleavage of a Lignin Model within a Cationic Metal-Organic Framework. *ACS Appl. Mater. Interfaces* **2021**, *13*, 688–695.
- (64) Islamoglu, T.; Goswami, S.; Li, Z.; Howarth, A. J.; Farha, O. K.; Hupp, J. T. Postsynthetic Tuning of Metal-Organic Frameworks for Targeted Applications. *Acc. Chem. Res.* **2017**, *50*, 805–813.
- (65) Deria, P.; Mondloch, J. E.; Tylilanakis, E.; Ghosh, P.; Bury, W.; Snurr, R. Q.; Hupp, J. T.; Farha, O. K. Perfluoroalkane Functionalization of NU-1000 via Solvent-Assisted Ligand Incorporation: Synthesis and CO₂ Adsorption Studies. *J. Am. Chem. Soc.* **2013**, *135*, 16801–16804.
- (66) Deria, P.; Bury, W.; Hupp, J. T.; Farha, O. K. Versatile Functionalization of the NU-1000 Platform by Solvent-Assisted Ligand Incorporation. *Chem. Commun.* **2014**, *50*, 1965–1968.
- (67) Deria, P.; Bury, W.; Hod, I.; Kung, C.-W.; Karagiari, O.; Hupp, J. T.; Farha, O. K. MOF Functionalization via Solvent-Assisted Ligand Incorporation: Phosphonates vs Carboxylates. *Inorg. Chem.* **2015**, *54*, 2185–2192.
- (68) Madrahimov, S. T.; Gallagher, J. R.; Zhang, G.; Meinhardt, Z.; Garibay, S. J.; Delferro, M.; Miller, J. T.; Farha, O. K.; Hupp, J. T.; Nguyen, S. T. Gas-Phase Dimerization of Ethylene under Mild Conditions Catalyzed by MOF Materials Containing (Bpy)NiII Complexes. *ACS Catal.* **2015**, *5*, 6713–6718.
- (69) Rimoldi, M.; Nakamura, A.; Vermeulen, N. A.; Henkelis, J. J.; Blackburn, A. K.; Hupp, J. T.; Stoddart, J. F.; Farha, O. K. A Metal-Organic Framework Immobilised Iridium Pincer Complex. *Chem. Sci.* **2016**, *7*, 4980–4984.
- (70) Baek, J.; Rungtaweeworant, B.; Pei, X.; Park, M.; Fakra, S. C.; Liu, Y.-S.; Matheu, R.; Alshimmri, S. A.; Alshehri, S.; Trickett, C. A.; Somorjai, G. A.; Yaghi, O. M. Bioinspired Metal-Organic Framework Catalysts for Selective Methane Oxidation to Methanol. *J. Am. Chem. Soc.* **2018**, *140*, 18208–18216.
- (71) Drache, F.; Cirujano, F. G.; Nguyen, K. D.; Bon, V.; Senkovska, I.; Llabrés i Xamena, F. X.; Kaskel, S. Anion Exchange and Catalytic Functionalization of the Zirconium-Based Metal-Organic Framework DUT-67. *Cryst. Growth Des.* **2018**, *18*, 5492–5500.
- (72) Lee, S.; Kapustin, E. A.; Yaghi, O. M. Coordinative Alignment of Molecules in Chiral Metal-Organic Frameworks. *Science* **2016**, *353*, 808–811.
- (73) Pei, X.; Bürgi, H.-B.; Kapustin, E. A.; Liu, Y.; Yaghi, O. M. Coordinative Alignment in the Pores of MOFs for the Structural Determination of N-, S-, and P-Containing Organic Compounds Including Complex Chiral Molecules. *J. Am. Chem. Soc.* **2019**, *141*, 18862–18869.
- (74) Yuan, S.; Lu, W.; Chen, Y.-P.; Zhang, Q.; Liu, T.-F.; Feng, D.; Wang, X.; Qin, J.; Zhou, H.-C. Sequential Linker Installation: Precise Placement of Functional Groups in Multivariate Metal-Organic Frameworks. *J. Am. Chem. Soc.* **2015**, *137*, 3177–3180.
- (75) Kapustin, E. A.; Lee, S.; Alshammari, A. S.; Yaghi, O. M. Molecular Retrofitting Adapts a Metal-Organic Framework to Extreme Pressure. *ACS Cent. Sci.* **2017**, *3*, 662–667.
- (76) Liao, P.-Q.; Li, X.-Y.; Bai, J.; He, C.-T.; Zhou, D.-D.; Zhang, W.-X.; Zhang, J.-P.; Chen, X.-M. Drastic Enhancement of Catalytic Activity via Post-Oxidation of a Porous MnII Triazolate Framework. *Chem. - Eur. J.* **2014**, *20*, 11303–11307.
- (77) Liao, P.-Q.; Chen, H.; Zhou, D.-D.; Liu, S.-Y.; He, C.-T.; Rui, Z.; Ji, H.; Zhang, J.-P.; Chen, X.-M. Monodentate Hydroxide as a Super Strong yet Reversible Active Site for CO₂ Capture from High-Humidity Flue Gas. *Energy Environ. Sci.* **2015**, *8*, 1011–1016.
- (78) Rieth, A. J.; Tulchinsky, Y.; Dincă, M. High and Reversible Ammonia Uptake in Mesoporous Azolate Metal-Organic Frameworks with Open Mn, Co, and Ni Sites. *J. Am. Chem. Soc.* **2016**, *138*, 9401–9404.
- (79) Lu, X.-F.; Liao, P.-Q.; Wang, J.-W.; Wu, J.-X.; Chen, X.-W.; He, C.-T.; Zhang, J.-P.; Li, G.-R.; Chen, X.-M. An Alkaline-Stable, Metal Hydroxide Mimicking Metal-Organic Framework for Efficient Electrocatalytic Oxygen Evolution. *J. Am. Chem. Soc.* **2016**, *138*, 8336–8339.
- (80) Rosen, A. S.; Mian, M. R.; Islamoglu, T.; Chen, H.; Farha, O. K.; Notestein, J. M.; Snurr, R. Q. Tuning the Redox Activity of Metal-Organic Frameworks for Enhanced, Selective O₂ Binding: Design Rules and Ambient Temperature O₂ Chemisorption in a Cobalt-Triazolate Framework. *J. Am. Chem. Soc.* **2020**, *142*, 4317–4328.
- (81) Oktawiec, J.; Jiang, H. Z. H.; Vitillo, J. G.; Reed, D. A.; Darago, L. E.; Trump, B. A.; Bernales, V.; Li, H.; Colwell, K. A.; Furukawa, H.; Brown, C. M.; Gagliardi, L.; Long, J. R. Negative Cooperativity upon Hydrogen Bond-Stabilized O₂ Adsorption in a Redox-Active Metal-Organic Framework. *Nat. Commun.* **2020**, *11*, 3087.
- (82) Rosen, A. S.; Notestein, J. M.; Snurr, R. Q. High-Valent Metal-Oxo Species at the Nodes of Metal-Triazolate Frameworks: The Effects of Ligand Exchange and Two-State Reactivity for C-H Bond Activation. *Angew. Chem., Int. Ed.* **2020**, *59*, 19494–19502.
- (83) Rieth, A. J.; Wright, A. M.; Skorupskii, G.; Mancuso, J. L.; Hendon, C. H.; Dincă, M. Record-Setting Sorbents for Reversible Water Uptake by Systematic Anion Exchanges in Metal-Organic Frameworks. *J. Am. Chem. Soc.* **2019**, *141*, 13858–13866.
- (84) Biswas, S.; Grzywa, M.; Nayek, H. P.; Dehnen, S.; Senkovska, I.; Kaskel, S.; Volkmer, D. A Cubic Coordination Framework Constructed from Benzobistriazolate Ligands and Zinc Ions Having Selective Gas Sorption Properties. *Dalton Trans.* **2009**, 6487–6495.
- (85) Denysenko, D.; Grzywa, M.; Tonigold, M.; Strepel, B.; Krkljus, I.; Hirscher, M.; Mugnaioli, E.; Kolb, U.; Hanss, J.; Volkmer, D. Elucidating Gating Effects for Hydrogen Sorption in MFU-4-Type Triazolate-Based Metal-Organic Frameworks Featuring Different Pore Sizes. *Chem. - Eur. J.* **2011**, *17*, 1837–1848.
- (86) Schmieder, P.; Denysenko, D.; Grzywa, M.; Baumgärtner, B.; Senkovska, I.; Kaskel, S.; Sastre, G.; van Wüllen, L.; Volkmer, D. CFA-1: The First Chiral Metal-Organic Framework Containing Kuratowski-Type Secondary Building Units. *Dalton Trans.* **2013**, *42*, 10786–10797.
- (87) Metzger, E. D.; Brozek, C. K.; Comito, R. J.; Dincă, M. Selective Dimerization of Ethylene to 1-Butene with a Porous Catalyst. *ACS Cent. Sci.* **2016**, *2*, 148–153.
- (88) Comito, R. J.; Fritzsche, K. J.; Sundell, B. J.; Schmidt-Rohr, K.; Dincă, M. Single-Site Heterogeneous Catalysts for Olefin Polymerization Enabled by Cation Exchange in a Metal-Organic Framework. *J. Am. Chem. Soc.* **2016**, *138*, 10232–10237.
- (89) Dubey, R. J.-C.; Comito, R. J.; Wu, Z.; Zhang, G.; Rieth, A. J.; Hendon, C. H.; Miller, J. T.; Dincă, M. Highly Stereoselective Heterogeneous Diene Polymerization by Co-MFU-4 L: A Single-Site

- Catalyst Prepared by Cation Exchange. *J. Am. Chem. Soc.* **2017**, *139*, 12664–12669.
- (90) Comito, R. J.; Wu, Z.; Zhang, G.; Lawrence, J. A.; Korzyński, M. D.; Kehl, J. A.; Miller, J. T.; Dincă, M. Stabilized Vanadium Catalyst for Olefin Polymerization by Site Isolation in a Metal-Organic Framework. *Angew. Chem., Int. Ed.* **2018**, *57*, 8135–8139.
- (91) Metzger, E. D.; Comito, R. J.; Wu, Z.; Zhang, G.; Dubey, R. C.; Xu, W.; Miller, J. T.; Dincă, M. Highly Selective Heterogeneous Ethylene Dimerization with a Scalable and Chemically Robust MOF Catalyst. *ACS Sustainable Chem. Eng.* **2019**, *7*, 6654–6661.
- (92) Park, H. D.; Comito, R. J.; Wu, Z.; Zhang, G.; Ricke, N.; Sun, C.; Van Voorhis, T.; Miller, J. T.; Román-Leshkov, Y.; Dincă, M. Gas-Phase Ethylene Polymerization by Single-Site Cr Centers in a Metal-Organic Framework. *ACS Catal.* **2020**, *10*, 3864–3870.
- (93) Denysenko, D.; Jelic, J.; Reuter, K.; Volkmer, D. Postsynthetic Metal and Ligand Exchange in MFU-4l: A Screening Approach toward Functional Metal-Organic Frameworks Comprising Single-Site Active Centers. *Chem. - Eur. J.* **2015**, *21*, 8188–8199.
- (94) Stubbs, A. W.; Dincă, M. Selective Oxidation of C-H Bonds through a Manganese(III) Hydroperoxo in Mn II -Exchanged CFA-1. *Inorg. Chem.* **2019**, *58*, 13221–13228.
- (95) Bien, C. E.; Chen, K. K.; Chien, S.-C.; Reiner, B. R.; Lin, L.-C.; Wade, C. R.; Ho, W. S. W. Bioinspired Metal-Organic Framework for Trace CO₂ Capture. *J. Am. Chem. Soc.* **2018**, *140*, 12662–12666.
- (96) Bien, C. E.; Liu, Q.; Wade, C. R. Assessing the Role of Metal Identity on CO₂ Adsorption in MOFs Containing M-OH Functional Groups. *Chem. Mater.* **2020**, *32*, 489–497.
- (97) Cai, Z.; Bien, C. E.; Liu, Q.; Wade, C. R. Insights into CO₂ Adsorption in M-OH Functionalized MOFs. *Chem. Mater.* **2020**, *32*, 4257–4264.
- (98) Mohamed, M. H.; Yang, Y.; Li, L.; Zhang, S.; Ruffley, J. P.; Jarvi, A. G.; Saxena, S.; Veser, G.; Johnson, J. K.; Rosi, N. L. Designing Open Metal Sites in Metal-Organic Frameworks for Paraffin/Olefin Separations. *J. Am. Chem. Soc.* **2019**, *141*, 13003–13007.
- (99) Li, L.; Yang, Y.; Mohamed, M. H.; Zhang, S.; Veser, G.; Rosi, N. L.; Johnson, J. K. Fundamental Insights into the Reactivity and Utilization of Open Metal Sites in Cu(I)-MFU-4 L. *Organometallics* **2019**, *38*, 3453–3459.
- (100) Röß-Ohlenroth, R.; Bredenkötter, B.; Volkmer, D. Organometallic MFU-4l(Arge) Metal-Organic Frameworks. *Organometallics* **2019**, *38*, 3444–3452.
- (101) Denysenko, D.; Grzywa, M.; Jelic, J.; Reuter, K.; Volkmer, D. Scorpionate-Type Coordination in MFU-4l Metal-Organic Frameworks: Small-Molecule Binding and Activation upon the Thermally Activated Formation of Open Metal Sites. *Angew. Chem., Int. Ed.* **2014**, *53*, 5832–5836.
- (102) Wright, A. M.; Sun, C.; Dincă, M. Thermal Cycling of a MOF-Based NO Disproportionation Catalyst. *J. Am. Chem. Soc.* **2021**, *143*, 681–686.
- (103) Wright, A. M.; Wu, Z.; Zhang, G.; Mancuso, J. L.; Comito, R. J.; Day, R. W.; Hendon, C. H.; Miller, J. T.; Dincă, M. A Structural Mimic of Carbonic Anhydrase in a Metal-Organic Framework. *Chem.* **2018**, *4*, 2894–2901.
- (104) Higashi, T.; Kusumoto, S.; Nozaki, K. Cleavage of Si-H, B-H, and C-H Bonds by Metal-Ligand Cooperation. *Chem. Rev.* **2019**, *119*, 10393–10402.
- (105) Habraken, E. R. M.; Jupp, A. R.; Brands, M. B.; Nieger, M.; Ehlers, A. W.; Slootweg, J. C. Parallels between Metal-Ligand Cooperativity and Frustrated Lewis Pairs. *Eur. J. Inorg. Chem.* **2019**, *2019*, 2436–2442.
- (106) Elsby, M. R.; Baker, R. T. Strategies and Mechanisms of Metal-Ligand Cooperativity in First-Row Transition Metal Complex Catalysts. *Chem. Soc. Rev.* **2020**, *49*, 8933–8987.
- (107) Brookes, M. J.; Jonathan, N. Infrared and Raman Spectra and Structures of Sodium Nitromethane and Sodium Trideuterionitromethane. *J. Chem. Soc. A* **1968**, 1529–1532.
- (108) Diel, B. N.; Hope, H. Convenient Synthetic Route to Coordination and Organometallic Compounds of Alkanenitronate [O₂N:CCR']⁻ Anions. *Inorg. Chem.* **1986**, *25*, 4448–4451.
- (109) Balogh-Hergovich, É.; Speier, G.; Huttner, G.; Zsolnai, L. Copper-Mediated Oxygenation of Nitronate to Nitrite and Acetone in a Copper(I) Nitronate Complex. *Inorg. Chem.* **1998**, *37*, 6535–6537.
- (110) Bittner, M. M.; Lindeman, S. V.; Fiedler, A. T. A Synthetic Model of the Putative Fe(II)-Iminobenzosemiquinonate Intermediate in the Catalytic Cycle of o-Aminophenol Dioxygenases. *J. Am. Chem. Soc.* **2012**, *134*, 5460–5463.
- (111) Matthews, W. S.; Bares, J. E.; Bartmess, J. E.; Bordwell, F. G.; Cornforth, F. J.; Drucker, G. E.; Margolin, Z.; McCallum, R. J.; McCollum, G. J.; Vanier, N. R. Equilibrium Acidities of Carbon Acids. VI. Establishment of an Absolute Scale of Acidities in Dimethyl Sulfoxide Solution. *J. Am. Chem. Soc.* **1975**, *97*, 7006–7014.
- (112) Bordwell, F. G. Equilibrium Acidities in Dimethyl Sulfoxide Solution. *Acc. Chem. Res.* **1988**, *21*, 456–463.
- (113) Parkin, G. Synthetic Analogues Relevant to the Structure and Function of Zinc Enzymes. *Chem. Rev.* **2004**, *104*, 699–768.
- (114) Gaillard, S.; Slawin, A. M. Z.; Nolan, S. P. A N-Heterocyclic Carbene Gold Hydroxide Complex: A Golden Synthone. *Chem. Commun.* **2010**, *46*, 2742–2744.
- (115) Boogaerts, I. I. F.; Nolan, S. P. Carboxylation of C-H Bonds Using N-Heterocyclic Carbene Gold(I) Complexes. *J. Am. Chem. Soc.* **2010**, *132*, 8858–8859.
- (116) Fortman, G. C.; Slawin, A. M. Z.; Nolan, S. P. A Versatile Cuprous Synthone: [Cu(IPr)(OH)] (IPr = 1,3 Bis-(Diisopropylphenyl)Imidazol-2-Ylidene). *Organometallics* **2010**, *29*, 3966–3972.
- (117) Tehranchi, J.; Donoghue, P. J.; Cramer, C. J.; Tolman, W. B. Reactivity of (Dicarboxamide)MII-OH (M = Cu, Ni) Complexes - Reaction with Acetonitrile to Yield MII-Cyanomethides. *Eur. J. Inorg. Chem.* **2013**, *2013* (22–23), 4077–4084.
- (118) Roşca, D.-A.; Smith, D. A.; Bochmann, M. Cyclometallated Gold(III) Hydroxides as Versatile Synthons for Au-N, Au-C Complexes and Luminescent Compounds. *Chem. Commun.* **2012**, *48*, 7247–7249.
- (119) Boogaerts, I. I. F.; Fortman, G. C.; Furst, M. R. L.; Cazin, C. S. J.; Nolan, S. P. Carboxylation of N-H/C-H Bonds Using N-Heterocyclic Carbene Copper(I) Complexes. *Angew. Chem., Int. Ed.* **2010**, *49*, 8674–8677.
- (120) Gascon, J.; Aktay, U.; Hernandez-Alonso, M. D.; van Klink, G. P. M.; Kapteijn, F. Amino-Based Metal-Organic Frameworks as Stable, Highly Active Basic Catalysts. *J. Catal.* **2009**, *261*, 75–87.
- (121) Kim, J.; Kim, Y. E.; Park, K.; Lee, Y. A Silyl-Nickel Moiety as a Metal-Ligand Cooperative Site. *Inorg. Chem.* **2019**, *58*, 11534–11545.
- (122) Kuznetsova, L. M.; Furer, V. L.; Maklakov, L. I. The Calculation of Absorption Curves in the IR Spectra of Free and Associated Methyl-N-Methylcarbamate Molecules. *J. Mol. Struct.* **1997**, *415*, 157–160.
- (123) Hwang, T. L.; Shaka, A. J. Water Suppression That Works. Excitation Sculpting Using Arbitrary Wave-Forms and Pulsed-Field Gradients. *J. Magn. Reson., Ser. A* **1995**, *112*, 275–279.
- (124) Walton, K. S.; Snurr, R. Q. Applicability of the BET Method for Determining Surface Areas of Microporous Metal-Organic Frameworks. *J. Am. Chem. Soc.* **2007**, *129*, 8552–8556.
- (125) Ohio Supercomputer Center, Columbus, OH, <http://www.osc.edu/> (accessed Jun 9, 2021).